ISSN: 1687-1006 p
ISSN: 2682-3640 e

The Egyptian International Journal of Engineering Sciences and Technology

https://eijest.journals.ekb.eg/

Vol. 47 (2024) 61–75

DOI: 10.21608/EIJEST.2024.250885.1253

Enhancing the Structural Performance of Wide Shallow Beams through Welded Stirrups: A Comprehensive Parametric Study and Experimental Validation

Azza I. Anan[a], Khaled Fawzy[b],Ahmed Moustafa[c*]

[a] Civil Engineering Department, High Institute for Engineering and Technology at Al-Obour (K21 Cairo /Bilbies Road), Higher Education Ministry, Cairo, Egypt.

[b] *Professor Structural Eng. Dept., Faculty of Eng., Zagazig University, Zagazig, Egypt.*
Vice Dean, High Institute for Engineering and Technology Al-Obour (K21 Cairo /Bilbies Road), Higher Education Ministry, Cairo, Egypt.

[c] *MSc student Structural Engineering, Faculty of Engineering, Zagazig University, Egypt.*

ARTICLE INFO

Article history:

Received 23 November 2023
Received in revised form 29 January 2024
Accepted 18 February 2024
Available online 18 February 2024

Keywords:

Shallow Wide Beam
Shear Reinforcement
Welded Stirrups

ABSTRACT

This study addresses the challenge of mitigating significant deflection in wide beams, resulting from their weak inertia in the load direction. Identifying deficiencies in both numerical and experimental methodologies, the research employs a parametric study to optimize enhancement techniques. The primary objective is a nuanced investigation into the impact of welded stirrups on the structural behavior of wide shallow beams, considering variations in stirrup spacing, stirrups welding, stirrup diameter, and compression steel ratio in comparison to tension reinforcement.

The research encompasses 10 specimens representing four enhancement factors, including three tested experimentally and seven through ANSYS models. One specimen undergoes both experimental and numerical representation for verification. The verification analysis, crucial for the intricate representation of welding in simulations, precedes a comprehensive comparison between experimental and numerical results, facilitating a holistic parametric study. The intricate representation of welding in ANSYS poses challenges due to the geometric, material, and thermal complexities associated with welding processes. Accurate modeling requires addressing nonlinear behavior, capturing residual stresses, and navigating multi-physics interactions, constituting a crucial yet intricate aspect in structural analysis.

All tested beams share identical dimensions: a clear span of 1800mm, width of 500mm, and thickness of 200mm. Experimental findings reveal a substantial enhancement in the load capacity of hidden beams, ranging from 54% to 62% when utilizing welded stirrups. Further analysis indicates that reducing stirrup spacing, diameter, and increasing compression steel ratio increases load capacity by 25.90%, 31.60%, and 49.19%, respectively.

The study extends its scrutiny to a comparison with international codes (ECP-203-2020, EN 1992, CSA2004, and ACI 318-14). The ratio between experimental shear force and calculated values from these codes varies from 0.85 to 3.79, providing crucial insights into the alignment or deviation of experimental results from global standards. This systematic exploration contributes valuable knowledge to the understanding and optimization of hidden beam performance.

1. Introduction

Addressing the architectural challenges of hidden beams in reinforced concrete structures has prompted researchers to explore solutions for mitigating issues

* Corresponding author. Tel.: +2-01272028223
E-mail address: Ahmed Moustafa.abdelkader@gmail.com

such as deflection. This introduction navigates through the intricacies of hidden beams, emphasizing their inherent challenges in the absence of infill walls, leading to unavoidable extensions beyond the ceiling. Various strategies, including the creation of 'hidden beams' by redistributing reinforcement within the slab [1], are discussed. The focus is on the need for additional measures to counteract the deflection observed in these structures.

To address significant deflection in wide shallow beams, researchers propose remedies such as adding a substantial percentage of compression steel reinforcement [2], increasing stirrups, or modifying concrete properties. Notably, enhancing beam properties, especially through stirrups designed to resist shear forces, has proven effective in deflection reduction. The strategic placement of stirrups in beams aligns with increased load-bearing capacity, resulting in diminished deflection.

Key influencing factors, such as loading type, material properties, and section properties, are explored in understanding deflection behavior [3]. Previous studies, exemplified by Irfan Nadagouda and G. Ravi [4], employed finite element modeling to simulate reinforced concrete slabs with hidden beams. Their work shed light on the relationship between concrete grade, deflection, and load-carrying capacity. The role of shear reinforcement, particularly stirrups, in controlling deflection is further examined in studies by Wayne Hsiung [5], Ata E. Shoeib [6], Mingzhe Cui [7], and Lele Sun [8].

Irfan Nadagouda and G.Ravi, 2017 [4] conducted a study involving finite element modeling of RC slabs featuring hidden beams and drop beams using ANSYS, a Finite Element (FE) method-based tool. The study revealed a close alignment between the behavior of RC slabs, as depicted by load-deflection curves in ANSYS, and experimental results. Slabs with hidden beams displayed higher deflection within the linear range before initial cracking, attributed to reduced cross-sectional area and stiffness. Concrete grade played a crucial role, with higher grades correlating with lower deflection. Comparative analysis demonstrated that slabs with drop beams exhibited a 26.63% analytical and 27.2% experimental increase in load-carrying capacity compared to hidden beams. FE analysis predicted slightly higher ultimate loads due to initial micro-cracks and instability issues in the experimental setup. The FE model's higher stiffness resulted in a 21.2% higher experimental deflection for slabs with hidden beams and 17.8% for slabs with drop beams compared to analytical deflection. Analytically, maximum deflection decreased by 32% for slabs with drop beams, attributed to increased stiffness and moment of inertia.

Wayne Hsiung [5] conducted a study on five models of large reinforced concrete beams with shear reinforcement, which were approximately one-third the size of the actual beams. The objective of the research was to examine the impact of different web widths and transverse stirrup distributions on the shear strength of beams. The results indicated that the ultimate shear capacity of beams increased proportionally with the width of the beam when the number of stirrups remained constant. Additionally, it was observed that the transverse distribution of stirrup legs across the web width had minimal influence on the shear capacity. When the stirrups were uniformly distributed across the web, the interior legs carried a higher shear force compared to the exterior legs.

Ata E. Shoeib [6] investigated the influence of shear reinforcement on the performance of wide shallow beams. The study sought to assess the effectiveness of various types of stirrups at different shear span-to-depth ratios (a/d) in enhancing the shear strength of shallow wide beams. The results indicated a significant improvement in the shear resistance of the tested shallow wide beams when using welded stirrups. A comparison between traditional stirrups (with four branches) and welded link stirrups demonstrated that the utilization of welded stirrups with thicknesses of 200mm and 150mm resulted in an increase in the ultimate load by approximately 31% and 16%, respectively, compared to regular stirrups.

Mingzhe Cui [7] performed monotonic and cyclic loading experiments to assess the effectiveness of welded reinforcement grids (WRGs), comprising smooth rebar, as shear reinforcement for reinforced concrete (RC) beams, in contrast to traditional bent smooth and deformed stirrups. The investigation concluded that WRGs exhibited satisfactory performance as shear reinforcement in RC beams, displaying comparable stiffness and ultimate capacity to conventional bent stirrups. Statistical analysis indicated no significant difference in normalized shear strengths between the test results obtained from the shear test database and the beams reinforced with WRG.

Lele Sun [8] examined the test results on the axial compression behavior of steel-reinforced concrete columns with welded stirrups (SRCC-WS). The study found that using welded stirrups for the confinement to concrete in SRCC-WS improved the ultimate axial compression strength by 7% and increased ductility by 10.5%, compared to traditional SRCC. However, the presence of longitudinal bars in SRCC did not effectively enhance the ultimate axial compression strength and ductility.

Khaled Fawzy & Mohamed A. Farouk [9] applied external lateral pressure along their spans through four angles placed at the beam corners and connected by

welded steel strips. This was done to study torsion strengthening of RC beams with external lateral pressure utilizing steel plates. The results revealed that the external lateral pressure strengthened the beams, resulting in improved torsional strength and performance compared to the control specimens and the specimens reinforced with external steel-reinforced beams. The rectangular beams, which were entirely and continuously encased with external steel, showed a notable improvement in torsional response. These beams' torsional capacities improved by about 171% and 44%, respectively, over those of the control specimen and the identical control specimen reinforced with the same external steel.

Khaled Fawzy [10] studied repair methods for corroded short reinforced concrete columns, and one of these methods involved the fusion welding of longitudinal bars into the external stirrups. The research findings indicated that welding longitudinal bars into the external stirrups of repaired columns enhanced the load-carrying capacity of the columns.

Finite element analysis (FEA) serves as a valuable approach to anticipate the structural response of materials and systems subjected to diverse loading conditions, eliminating the necessity for extensive experimental endeavors. Several researchers have utilized FEA to scrutinize the shear performance of steel stirrups in reinforced concrete beams, validating its precision through comparisons with experimental findings [11].

This study aims to contribute to the existing body of knowledge by specifically investigating the impact of stirrup-related parameters, such as spacing, welding, diameter, and compression steel ratio, on enhancing the resistance to deflection in hidden beams. Through a thorough exploration of these factors, this research seeks to provide valuable insights for the design and construction of reinforced concrete structures with hidden beams.

2. Experimental Program

2.1. Materials

All mixes in the study used ordinary Portland cement with a grade of 52.5 N/mm^2, which was manufactured by the Sinai Cement Factory and complied with ESS 4756-1-2006 [12]. Drinkable clean tap water was used for mixing. The fine aggregate utilized in the study consisted of natural siliceous sand, which was free from harmful substances and relatively clean. The coarse aggregate employed consisted of naturally crushed stone (Dolomite) with a fineness modulus measuring 3.93, exhibiting a water absorption rate of 0.94%, and possessing a maximum nominal size of 20 mm.

In this research, two categories of steel were utilized for reinforcing the concrete. The first category was mild steel bars with a diameter of 8 mm, which had a yield strength of 240 MPa and were utilized as shear reinforcement. The second category was deformed high tensile strength bars exhibiting a yield strength of 420 N/mm^2 and diameters of 12 and 16 mm, which were used as top and bottom reinforcement, respectively. “Figure 1“illustrates the arrangement of these bars.

Fig. 1. Steel Cage

2.2. Mix proportion and testing of specimens

An experimental program was conducted to investigate the impact of welded stirrups on the performance of reinforced concrete (RC) hidden beams and to assess their deflection values under various parameters. The program included three simply supported RC hidden beams, each having a width of 500mm, a length of 1800mm, and a thickness of 200mm. The beams were reinforced with four bottom longitudinal bars of 16mm diameter and four top bars of 12mm diameter, as shown in “Table 1“.

Table 1: Beam models

Traditional stirrups	Welded stirrups
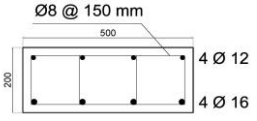 a) FS101	
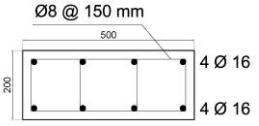 b) CS402	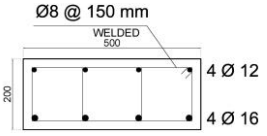
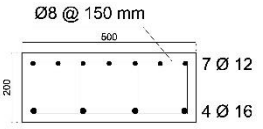 c) CS403	h) BS701
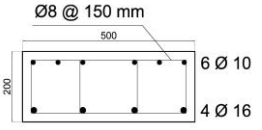 d) CS404	

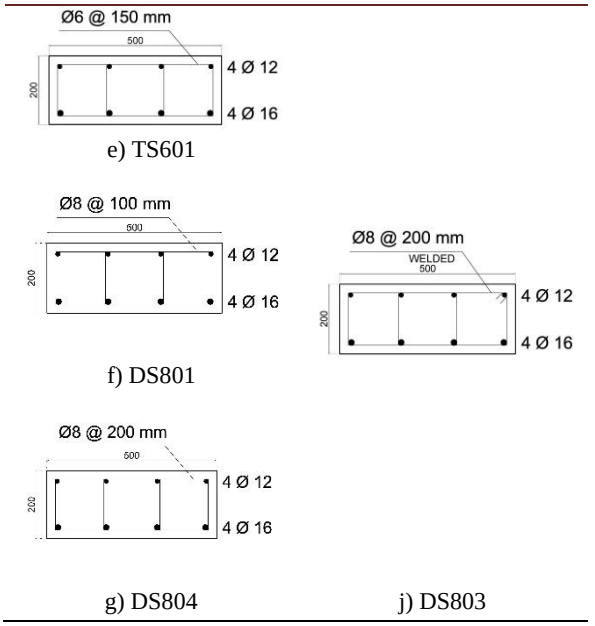

There are two types of stirrups used in the tested beams, as shown in "Table 1". The first type of beams contained traditional stirrups with four branches Ø 8mm @ 150 mm (FS101) for verifying the model ANSYS and studying its contribution for the load capacity and deflection of hidden beam, while the second type contained four branches welded stirrups Ø 8mm with the top and bottom longitudinal reinforcement, the second type had two tested beams, BS701 and DS803 having spacing 150 and 200 mm respectively to study the welding effect and stirrups spacing effect. Welding was performed at the intersections of the stirrups with the upper and lower reinforcement steel, as shown in "Figure 2".

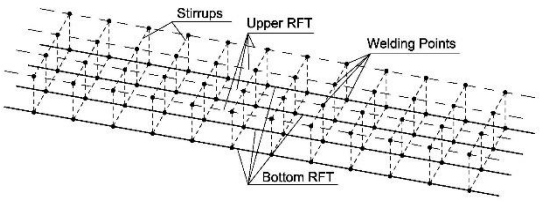

Fig. 2. Welding of stirrups process and places

The concrete mixture was formulated to achieve a desired compressive strength of 35 MPa at the end of 28 days. The design of the concrete mix followed the absolute volume method, as shown in "Table 2", to reach the required strength and it was supplied with the required quantities and proportions from a ready-mix concrete station to ensure that all specimens had the same concrete strength. A mechanical vibrator was used to ensure that there was no honeycomb in the concrete. The beams were cast as in "Figure 3", and also 3 cubes and 3 cylinders. The beams, cubes, and cylinders were treated with water for 28 days. After 28 days, a compressive test was done for cubes and cylinders and a Brazilian test of tensile strength for 1 cylinder as in "Figure 4"to find out the strength of the concrete used.

Table 2: Concrete mix proportions

dolomite	Sand	Cement	Water
2.80	1.80	1.00	0.45

Fig. 3. Pouring concrete for beam specimen

Fig. 4. Testing and pouring concrete for cubes and cylinder specimens

3. Test Measurements and Instrumentation

The beams were subjected to testing using a manually operated hydraulic jack with a 3000kN capacity, manually operated by an oil pump.

The experimental arrangement and equipment used can be observed in "Figure 5". A digital load indicator

connected to an electrical load cell with a precision of 0.1 kN was employed to measure the vertical loads applied. The specimens were loaded using a three-point regime, with a jack applying the load at a single point located in the middle of the beam, which was supported by two steel beams representing the support points. The deflection of the beams was monitored at the mid-span position. The load cell was connected to a data acquisition system, which was then connected to a computer for data recording and analysis. The data acquisition system was responsible for the continuous recording of the load and displacement of the beams throughout the testing process until failure. The load is increased by a fixed amount every second, and the corresponding amount of deflection is measured until the breakdown, and the device records the force for each second and the corresponding deflection. Then the curves were drawn for the points extracted from the device. The cracks were identified and monitored at each load step until failure occurred. At the same time, the load causing the first visible cracks and the amount of deflection were noted.

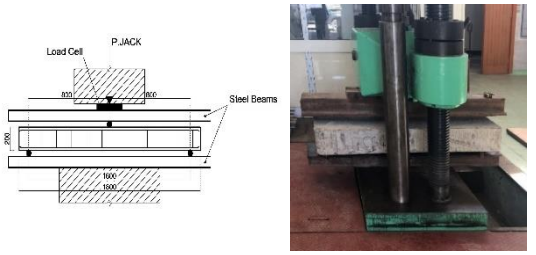

Fig. 5. Test arrangement and instrumentation of tested beams

4. Test Results and Analysis

4.1. Crack Pattern and Mode of Failure

The crack patterns of all specimens subjected to testing are illustrated in "Figure 6". In general, it was noticed that the initial crack (P_{cr}) was a vertical flexural crack that developed close to the mid-span. Additional diagonal cracks then started to develop, spread horizontally, and headed either for the top compression face or the bottom. The maximum failure load (P_{max}) is listed in "Table 3". The cracking loads observed in the experiments varied from 54% to 62% of the maximum loads. The comparison between traditional stirrups and welded stirrups indicated that the use of welded stirrups had a positive effect on both the cracking load and the maximum failure load, resulting in an increase.

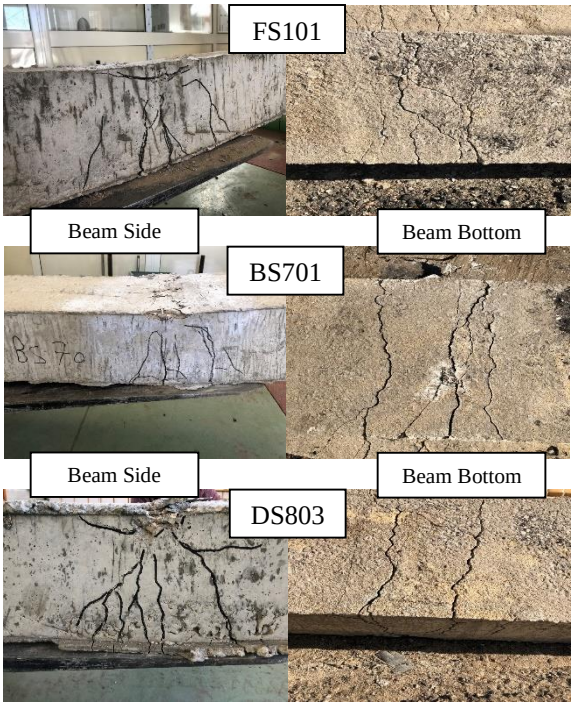

Fig. 6 Crack pattern of tested beams

4.2. Load Deflection Curves

The load-deflection curves, are shown in "Figure 7", illustrate the response at the mid-span of the specimens. Overall, the incorporation of welded stirrups substantially mitigated deflection, leading to an augmentation in the maximum failure load of the tested specimens and an enhancement in structural behavior.

Table 3: The results of the tested specimens.

Specimens	Type of stirrups	Spacing of stirrups	F_{cu} (MPa)	P_{cr} (kN)	P_{max} (kN)	P_{cr}/P_{max}	Def. at P_{max} (mm)	Def. reduction ratio compared to FS101
FS101	Traditional	Ø 8@150 mm	35.88	80.87	149.77	0.54	39.2	0%
BS702	Welded	Ø 8@150 mm	35.88	96.20	155.16	0.62	19.4	50.50%
DS801	Welded	Ø 8@200 mm	35.88	94.66	155.18	0.61	20.7	47.20%

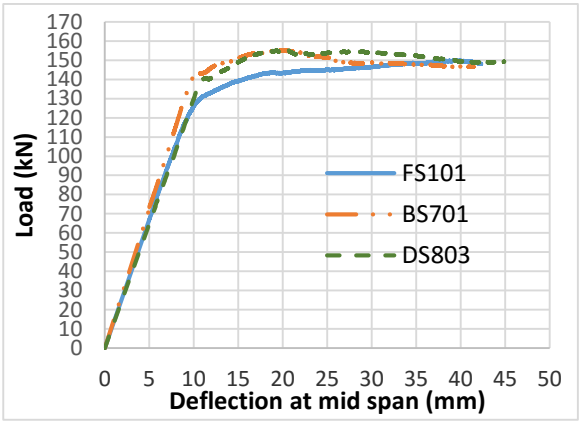

Fig. 7. Type of stirrups impact on the load-deflection curves

As shown in "Table 3" and "Figure 7 the superior performance of beams with welded stirrups in reducing deflection and supporting loads is evident compared to those without welded stirrups. The utilization of welded stirrups results in a significantly lower deflection value, creating an interconnected system with the reinforcement (RFT) on both the compression and tension sides. This collaborative action enhances the beam's ability to withstand loads. For instance, at the maximum load of 149.77 kN sustained by the FS101 beam, the deflection is 39.2 mm. In contrast, beams BS701 and DS803, both utilizing welded stirrups, exhibit deflections of 14 mm and 15.3 mm, respectively, under the same load. This underscores the considerable impact of welded stirrups, reducing deflection by approximately 50.50% and 47.20% for tested beams BS702 and DS801, respectively, in comparison to beams without welded stirrups (FS101). This indicates a noteworthy improvement in beam efficiency, with a reduction in deflection exceeding 50%. At the maximum deflection, specimen FS101 sustains a load of 149.77 kN, while specimens BS701 and DS803 support loads of 155.16 kN and 155.18 kN, respectively. This suggests an efficiency increase of about 5.20% and 5.30% in load-bearing capacity relative to the beam without welded stirrups (FS101). Consequently, the utilization of welded stirrups significantly enhances shear resistance in RC hidden beams. A comparison between traditional and welded stirrups underscores the latter's superior effectiveness in reducing deflection. Despite the increase in the distance between the stirrups and their welding, it has a better effect than the traditional stirrups in the FS101 specimen, although the distances between the stirrups are less.

5. Theoretical Investigation Utilizing Finite Element Software (ANSYS)

5.1. Methodology for Finite Element Modelling and Analysis Using ANSYS

The Finite Element Analysis (FEA) is a technique that is utilized to assess structures by predicting the response of their components to different loads accurately. FEA is a preferred method for studying the behavior of structural components as it is quicker and more cost-effective than experimental methods. Although the finite element method is an approximate technique, the accuracy of the solution is significantly influenced by the number of elements used in a model.

To simulate the beam in ANSYS, a solid element (SOLID65) was used for concrete, a Link 180 for reinforcement steel bars, and a SOLID185 for steel plate, as shown in "Figure 8". All beams in the investigation were modeled as simply supported beams, with the left support constrained in both vertical and horizontal directions (Uy and Ux), and the right support restricted to vertical movement only (Uy), functioning as a roller support. The analysis was performed as a static analysis with small displacements. The time value for ANSYS to correspond with the boundary conditions after the load step is termed the time at the end of the load step.

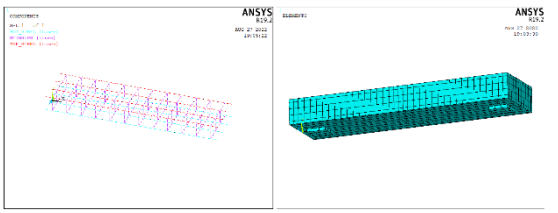

Fig. 8. Modelling of the tested beams (ANSYS 2019) [13]

In order to ensure the accuracy and validity of the finite element model, a verification process is conducted on the experimental control specimen using various factors. In the theoretical specimens, the bond between the concrete and steel reinforcement is assumed to be ideal in the finite element models.

5.1.1. Structural Material Modelling

The following elements have been adopted for material idealization,

5.1.1.1. Concrete Idealization:

The analysis of reinforced concrete behavior is carried out using the SOLID65 element, which has a

hexahedral shape with three translational degrees of freedom in x, y, and z directions "Figure 9". This element is designed to simulate plastic deformation, and cracking in three orthogonal directions at each integration point of the concrete material. The constitutive model used for the triaxial behavior of concrete is based on the element's ability to change its stiffness matrices. In case the concrete at an integration point is subjected to uniaxial, biaxial, or triaxial compression, it is considered crushed at that specific point.

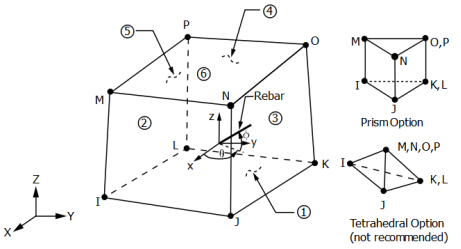

Fig. 9. Geometry of SOLID65 element (ANSYS 2019) [13]

Creating a model to depict the behavior of concrete can be a difficult task. The shear transfer coefficient typically ranges from 0.0 to 1.0, where 0.0 represents a smooth crack, which results in complete loss of shear transfer, and 1.0 represents a rough crack, which results in no loss of shear transfer. To deactivate the crushing capability of the concrete element, the uniaxial crushing stress is inputted as -1. The modulus of elasticity and uniaxial tensile cracking stress of concrete are obtained using IS 456:2000, and the multi-linear isotropic properties of concrete's stress-strain behavior are inputted. Poisson's ratio is assumed to be 0.2. The shear transfer coefficients for open and closed cracks are 0.3 and 0.9, respectively.

5.1.1.2. Steel reinforcement idealization:

The LINK180 element is utilized for simulating the behavior of the steel reinforcement in the RC beam. This element is a 3D spar element "Figure 10" that is widely used in different engineering applications. It is adept at handling plasticity, creep, swelling, stress stiffening, and large deflections. Each node of the element possesses three degrees of freedom translations in the nodal x, y, and z directions. Notably, this element is not designed to bear bending loads. The steel reinforcement in the RC beam is Fe500, and the assumed elastic modulus and Poisson's ratio for all reinforcing bars are 2.1×10^5 N/mm^2 and 0.3, respectively. To prevent instability after yielding, a tangent modulus of 20 N/mm^2 is employed for reinforcement. Uniform stress distribution across the entire element is assumed.

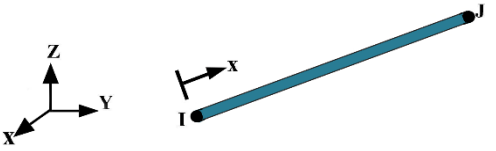

Fig. 10. Geometry of LINK180 element (ANSYS 2019) [13]

5.1.1.3. Idealization of Reinforcement in Concrete:

The way in which steel reinforcement is included in concrete depends on the system's geometry, and this can be done using discrete, embedded, or smeared models. The method used in this paper to model the reinforcement is discrete modeling. This technique as shown in "Figure 11", entails linking spar or beam elements with properties that align with those of the initial reinforcing elements to the nodes of the concrete mesh. Consequently, the nodes are shared between the concrete and reinforcement meshes, and the concrete occupies identical regions as the reinforcement.

The discrete modeling approach is considered to be an accurate and realistic representation of the actual field conditions for RC beams with clearly defined geometry and reinforcement details. Hence, this approach has been employed in the current investigation, and the findings have been documented.

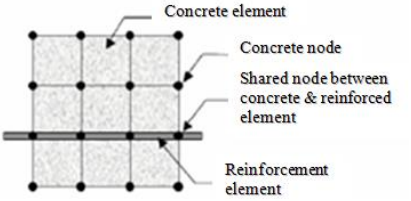

Fig. 11. Discrete reinforcement modeling for reinforced concrete (Tavarez, 2001) [14]

5.1.1.4. Idealization of Steel Plates:

Solid185 components are used to simulate the steel plates at the beam supports. Solid185 is well-suited for modeling general 3-D solid structures, accommodating prism and tetrahedral degenerations in irregular regions. It supports various element technologies, including B-bar, uniformly reduced integration, and enhanced strains.

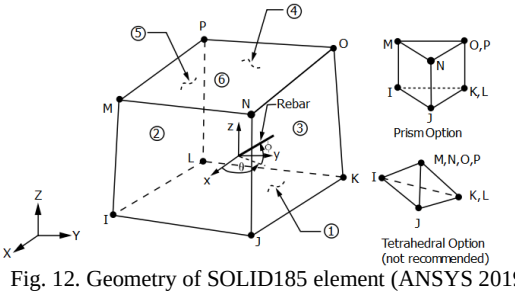

Fig. 12. Geometry of SOLID185 element (ANSYS 2019) [13]

5.1.2. Material properties

5.1.2.1. Concrete

Developing a concrete behavior model is intricate due to its quasi-brittle nature and distinct compression and tension responses. Concrete's tensile strength is generally 8-15% of its compressive strength [15]. "Figure 13" provides a representation of the typical stress-strain curve for normal-weight concrete [16].

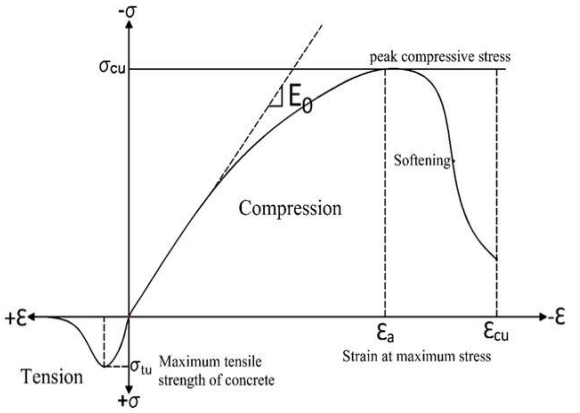

Fig. 13. Typical uniaxial compressive and tensile stress-strain curve for concrete (Bangash 1989) [16]

Concrete's stress-strain curve exhibits linearly elastic in compression up to around 30% of its maximum compressive strength. Beyond this threshold, the stress increases gradually until reaching the maximum compressive strength σ_{cu}. Subsequently, the curve descends into a softening region, culminating in crushing failure at an ultimate strain ε_{cu}. In tension, the stress-strain curve for concrete is approximately linearly elastic up to the maximum tensile strength. Following this point, the concrete undergoes cracking, leading to a gradual decrease in strength until reaching zero [16].

The ANSYS program necessitates the uniaxial stress-strain relationship for concrete under compression. Numerical expressions [17], denoted as Equations (a) and (b), were applied in conjunction with Equation (c) [18] to formulate the uniaxial compressive stress-strain curve for concrete in this investigation. The simplified compressive uniaxial stress-strain relationship utilized in this study is illustrated in "Figure 14".

$$f = \frac{E_c \varepsilon}{1 + \left(\frac{\varepsilon}{\varepsilon_0}\right)^2} \quad \text{(a)}$$

$$\varepsilon_0 = \frac{2 f'_c}{E_c} \quad \text{(b)}$$

$$E_c = \frac{f}{\varepsilon} \quad \text{(c)}$$

Where; f_c : Stress at any strain ε.

ε_o: Strain at the ultimate compressive strength.

E_c: Elastic modulus (E_c).

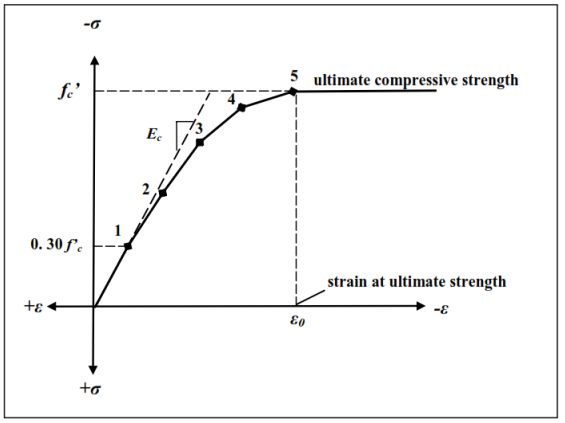

Fig. 14. Concrete's simplified compressive uniaxial stress-strain curve (Gere and Timoshenko 1997) [18]

5.1.2.2. Steel

The steel material in the finite element models was presumed to exhibit elastic-perfectly plastic behavior and to be identical in tension and compression, as shown in "Figure 15". A Poisson's ratio of 0.3 was employed for the steel reinforcement in this investigation.

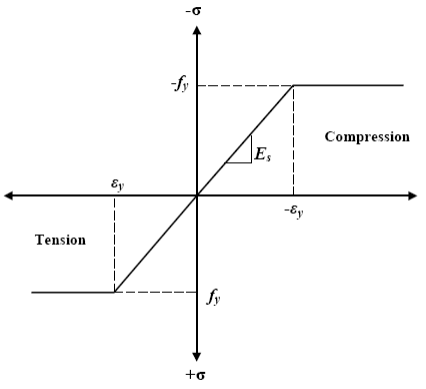

Fig. 15. Stress-strain relation for reinforcement steel

5.1.3. Model convergence study:

The seven modeled specimens are divided into four groups with the different studied parameters as shown in “Figure 16”. In the first group, one modeled specimen named "FS101" with traditional stirrups was tested with the 200mm thickness for verification of the model with experimental results. In the second group, the three modeled specimens with different upper reinforcements named "CS402", "CS403" and "CS404" presented the compression steel parameter. In the third group, one modeled specimen with 6mm steel stirrups named "TS601" presented the stirrups diameter parameter. In the fourth group, two modeled specimens with different stirrups spacing named "DS801" and "DS804" presented the stirrups spacing parameter.

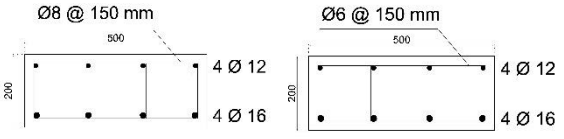

a) FS101 Specimen b) TS601 Specimen

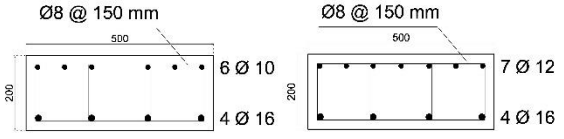

d) CS404 Specimen e) CS403 Specimen

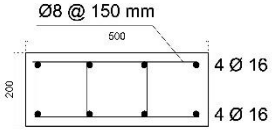

f) CS402 Specimen

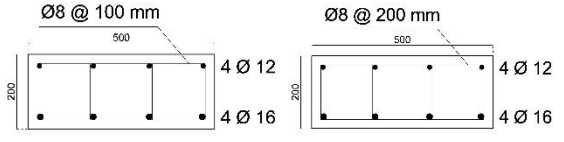

g) DS801 Specimen h) DS804 Specimen

Fig. 16. Beam models with different reinforcement

A static nonlinear analysis is considered for the study under transverse incremental loading to study the flexural behavior (Load deflection behavior, load carrying capacity, and crack patterns) of beams, by simulating the experimental work analytically. ANSYS employs “Newton-Raphson” method to solve nonlinear problems, which is a method that involves an iterative process to solve a nonlinear or complex problem.

5.2. Experimental and Numerical Verification

“Figure 17” shows the load-deflection curves of the analytical tested specimens and the experimental specimen FS101. The findings suggest that the theoretical stiffness is greater than the experimental stiffness because the assumed full bond between the steel and concrete in the theoretical model prevents any slippage, which is not accounted for in the experimental work. Moreover, the FE model did not consider the small cracks that occurred in the tested beams due to dry shrinkage. And due to the difference in the boundary condition between the theoretical model and the experimental specimen, as in the lab, the edges of the beam are free to move from the top, meaning that they are not completely fixed as achieved in the theoretical specimen.

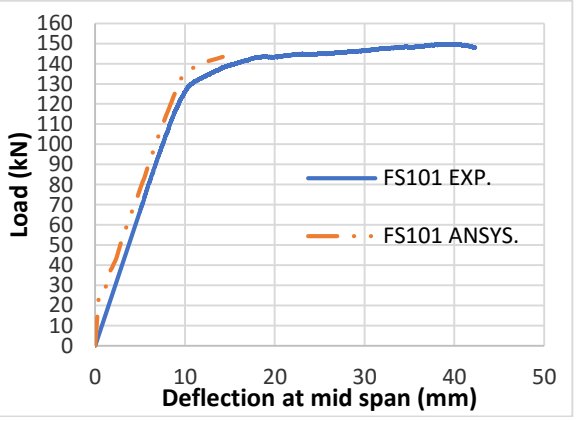

Fig. 17. Comparison between theoretical load-deflection curve and experimental

5.3. Finite Element Results & Discussions

The analytical results are obtained for beams with different parameters. The deflection (Def.) corresponding to the incremental load is obtained at the center of the beam. Ultimate load & the crack patterns are obtained, and they are discussed as follows:

5.3.1. Comparison of Load- deflection Behavior

The final load in the finite element model corresponds to the final applied load step before the solution diverges, primarily attributed to the presence of multiple cracks and extensive deflections. The ultimate load of all the specimens obtained from FE analysis is shown in “Table 4”.

Table 4: ANSYS Results.

Specimens	Def. at $P_{118\ kN}$ (mm)	Def. at $P_{118\ kN}$ reduction ratio compared to FS101	P_{max} (kN)	Def. at P_{max} (mm)	Def. reduction ratio compared to FS101
FS101	8.28	0.00%	143.38	14.21	0.00%
CS402	7.22	12.80%	118.1	7.22	49.19%
CS403	7.17	13.41%	137.72	9.14	35.68%
CS404	8.22	0.72%	143.24	13.27	6.62%
TS601	7.35	11.23%	139.04	9.72	31.60%
DS801	7.82	5.56%	142.90	13.56	4.57%
DS804	8.58	-3.62%	136.55	10.53	25.90%

The ANSYS V19 software was utilized to monitor the stress distribution on the tested beam in the finite element model at each load step [13]. The beam failure mode in the experiment was a flexural failure, which was consistent with the actual failure mode. The failure load and mid-span deflection were obtained from the data file. The maximum load from the finite element analysis is presented in "Table 4", while "Figures 18–21" compare the load-deflection curves for the finite element models.

To ensure a fair comparison, the deflection for all samples was compared at the same load, which is 118 kN, the maximum load that the TS601 specimen can withstand. This allows us to accurately and satisfactorily deduce the percentage of change.

As shown in the figures, there is a significant enhancement in hidden beams while increasing the compression steel ratio, reducing stirrups diameter, or reducing stirrups spacing .The enhancement can be observed from the curves, where we notice that the deflection is less compared to the main model FS101, but this change is slighter than the experimental specimens, as previously mentioned there was a significant enhancement in the hidden beams experimented in the lab.

5.3.1.1. The Effect of Compression RFT

According to "Figure 18" and deflection values at P_{max} in "Table 4", the efficiency of the beam increases by a great percentage when the compression RFT is increased, as we note that in the default model, we use upper RFT 4@12 which represents 56% of the tension RFT as in model FS101 and when this percentage is increased to become 100%, meaning that the RFT in compression and tension are the same as in model CS402 we notice an increase by 49.19% in the efficiency of the beam, but when using the same percentage of reinforcement, but with a smaller diameter, to find out whether the diameter and number have an effect, such as model CS403, we see that the effect is less than model CS402, but we notice a 35.68% increase in the efficiency of the beam than default model, and similarly to model CS404, the same reinforcement ratio for specimen FS101 was used, but With a larger number and less diameter, and we note from "Figure 18" that the effect is almost unnoticeable and it was 6.62%.

But as mentioned earlier, the comparison will be conducted at a load of 118 kN to ensure an accurate comparison. We find that the increase in the efficiency of specimen CS403 is 13.41%, which is higher than the improvement percentage of specimen CS402, which is 12.80%. This is evident from the curve, which shows that the deflection results for specimen CS403 are slightly better than those for specimen CS402. Therefore, distributing the reinforcement ratio over a greater number, by reducing the diameter, provides better improvement than reducing the number of bars and increasing the diameter.

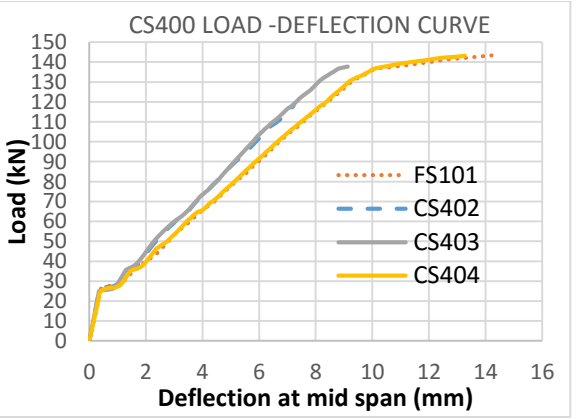

Fig. 18. Load-deflection for specimens with different compression RFT

5.3.1.2. The Effect of Stirrups Diameter

According to "Figure 19" and deflection values at P_{max} in "Table 4", the efficiency of the beam increases by 31.60% compared with the default model FS101 when using 6 mm diameter stirrups instead of 8 mm as in model TS601, but the default model continues to sustain loads more than loads of model TS601 as shown in the figure.

Logically, reducing the diameter of the stirrups would decrease the capacity load of the specimen, resulting in larger deflection values compared to the default specimen FS101. However, from the observed results, the beam's capacity was enhanced, and deflection results were significantly better. This raises

the question of why the results improved despite the reduction in stirrups' diameter. This question cannot be answered through the examination of a single specimen. It opens the door for further investigation into this variable in future studies.

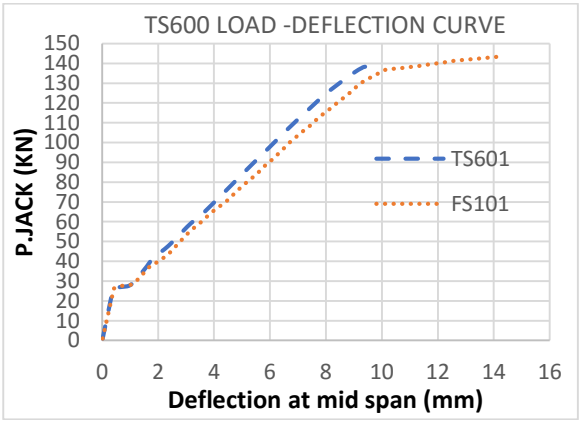

Fig. 19. Load-deflection for specimens with different Stirrups diameter

5.3.1.3. The Effect of Stirrups Spacing

According to "Figure 20" and deflection values at P_{max} in "Table 4", in the default model FS101, 8 mm diameter stirrups were placed at 150 mm spacing. When the spacing between the stirrups was reduced to 100 mm, as in the DS801 model, the efficiency of the beam increased by 4.57%, and when the spacing between the stirrups was increased to 200 mm, as in the DS804 model, we see that the efficiency of the beam increases by 25.90% compared with the default model FS101. But this comparison is unfair because we comparing the deflection values at the max load for each sample which varies from one sample to another, as we see in "Figure 20" sample DS801 has greater results than samples FS101 and DS804.

This is also evident from Table 4 that the deflection values at the comparison load of 118 kN show a significant enhancement for specimen DS801 by 5.56% compared to the default specimen FS101. On the other hand, specimen DS803 exhibited a negative improvement ratio of -3.62%, indicating a reduction in beam efficiency compared to the default specimen. Thus, we can conclude that reducing the spacing between the stirrups is a key factor contributing to the enhancement of the efficiency of hidden beams, regardless of the magnitude of the deflection at the maximum load. This is because the maximum load varies for each specimen, making it inappropriate to judge the specimens solely based on the maximum load and its corresponding deflection.

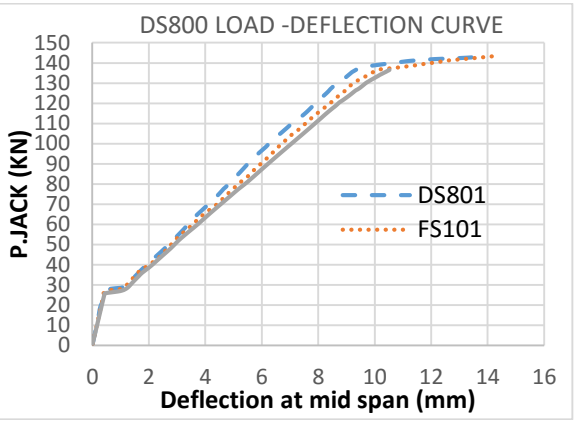

Fig. 20. Load-deflection for specimens with Stirrups spacing

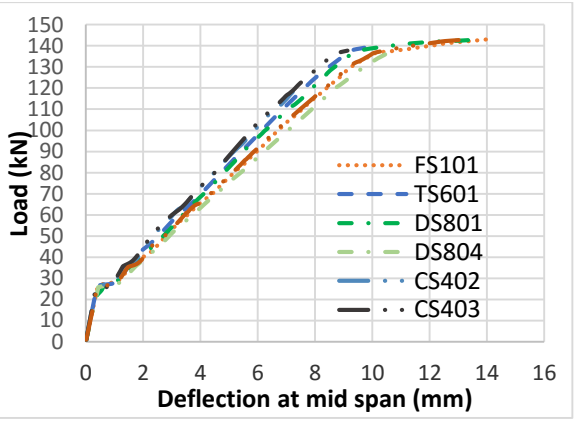

Fig. 21. Load-deflection for all FE specimens

5.3.2. Crack pattern:

During the FE analysis, various concrete crack patterns were generated to examine the different types of cracks that occurred within the concrete at different load steps. The ANSYS program kept track of the crack pattern at each load step. The obtained crack patterns from the analytical study are quite similar to the crack patterns observed during the experimental study as shown in "Figure 22".

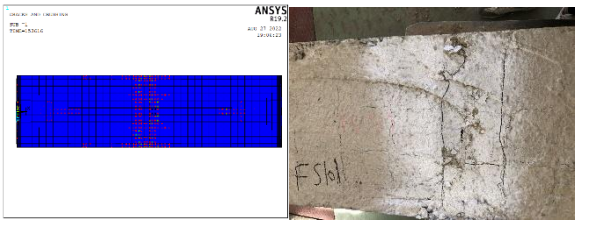

Fig. 22. Comparison between theoretical and experimental specimen cracks

6. Comparing Experimental and Analytical Ultimate Load Across Various Codes

The impact of vertical stirrups is not taken into account for RC beams with a depth of less than 250mm according to ECP 203-2020 [19]. However, ACI 318-14 [20], CSA 2004 [21], and EN1992 [22] consider the contribution of shear reinforcement using equations 1, 2, and 3, respectively.

$$V_s = \frac{A_{st}\, x\, {}^{f_y}/_{\gamma_s} xd}{S} \qquad (1)$$

$$V_s = \frac{A_{st}\, f_y d_v x \cot\theta}{S} \qquad (2)$$

A_{st}, or A_v = area of shear reinforcement (mm^2); Θ= Angle of inclination of the diagonal compressive struts;

$$V_{RD} = V_{RD,s} = \frac{A_{sw}}{S} xZx f_{ywd} x \cot\theta \le V_{RD,max} = \frac{a\, xv_1 x f_{cd}}{\cot\theta + \tan\theta} xbxZ \qquad (3)$$

A_{sw} = cross-sectional area of the shear reinforcement (mm^2), S = spacing of the stirrups (mm); f_{ywd} = yield strength of the shear reinforcement (MPa) for vertical shear reinforcement; Θ= angle between compression strut and the longitudinal axis; equal to 45°; z = the inner lever arm for a member with constant depth (mm).

The shear resistance obtained from experimental, FEA models, and numerical calculations using ECP 203-2011, ACI 318-14, EN1992, and CSA 2004 are compared in "Table 5", with the inclusion of stirrup contribution in the shear resistance.

The results in "Table 5" demonstrate that all codes tested produced conservative outcomes. Moreover, the ratio between the experimental shear force and the one calculated using ECP-203, while taking into account the vertical stirrups contribution, ranges from 1.46 to 3.79.

Table 5: Comparison between the experimental shear forces with stirrups and predicted by different codes.

Specimens	Experimental shear capacity		V_{FEA} / $V_{exp.}$	Predicted Shear Capacity "$V_{code.}$" (kN)							
				ECP203-2011		ACI 318-14		EN-1992		CSA-2004	
	$V_{exp.}$ (kN)	V_{FEA} (kN)		V_{code} (kN)	V/ V_{code}	V_{code} (kN)	V/ V_{code}	V_{code} (kN)	V/ V_{code}	V_{code} (kN)	V/ V_{code}
FS101	74.885	71.69	95.57%	32.64	2.20	48.95	1.46	48.25	1.49	56.30	1.27
CS402	---	59.05	---	32.64	1.81	48.95	1.21	48.25	1.22	56.30	1.05
CS403	---	68.86	---	32.64	2.11	48.95	1.41	48.25	1.43	56.30	1.22
CS404	---	71.62	---	32.64	2.19	48.95	1.46	48.25	1.48	56.30	1.27
TS601	---	69.52	---	18.36	3.79	27.54	2.52	27.14	2.56	31.67	2.20
BS701	77.58	---	---	32.64	2.38	48.95	1.58	48.25	1.61	56.30	1.38
DS801	---	71.45	---	48.95	1.46	73.43	0.97	72.38	0.99	84.45	0.85
DS803	77.59	---	---	24.48	3.17	36.72	2.11	36.19	2.14	42.22	1.84
DS804	---	68.28	---	24.48	2.79	36.72	1.86	36.19	1.89	42.22	1.62

6.1. Calculating Enhancement Factor from Deflection Equation

According to different codes the deflection can be calculated by one equation according to the shape of the load, its location, and support condition for our case we have a simple beam with a concentrated load at the middle of the span, and the equation to calculate the deflection for our case as the following:

$$\Delta = \frac{1}{48}\frac{PL^3}{EI}$$

Where Δ=Deflection (mm), P=concentrated load value (N), L=length of the beam (mm), E= modulus of elasticity (N/mm^2)**,** and I=moment of inertia (mm^4).

From the previous equation (L) and (I) are constant for all beams as we use the same beam dimension for all samples, also (E) value is constant because we use the same material for all samples so we can simplify the equation to the following:

$E=220000\ N/mm^2$,
$I=bh^3/12=500*200^3/12=3.33*10^8\ mm^4$,and
$L=1800mm$

By substituting into the equation

$$\Delta = \frac{1}{48}\frac{PL^3}{EI} = \frac{P}{60356.653} \rightarrow P_{(kN)} = 60.357\,\Delta_{(mm)}$$

From this equation, we found that there is a direct relation between load and deflection as whenever the load is increased the deflection also increased and we can consider that the value 60.357 is a constant for our case and equal (C)

So $P_{(kN)} = C\,\Delta_{(mm)}$

From curves that were exported from ANSYS and experimental work for each parameter we exported an equation for each curve between load and deflection by using Microsoft Excel, the exported equations are presented in "Table 6":

Table 6: Comparison between enhancement factors for all samples.

Specimens	Analysis Type	Exported Equation from Curves $P_{(kN)} = X\,\Delta_{(mm)}$	X=C/K	K
FS101	Experimental	P=12.994 Δ	12.994	4.645
FS101	ANSYS	P=12.516 Δ	12.516	4.822
CS402	ANSYS	P=14.20 Δ	14.20	4.251
CS403	ANSYS	P=13.907 Δ	13.907	4.34
CS404	ANSYS	P=12.513 Δ	12.513	4.823
TS601	ANSYS	P=13.356 Δ	13.356	4.519
BS701	Experimental	P=14.478 Δ	14.478	4.169
DS801	ANSYS	P=13.409 Δ	13.409	4.501
DS803	Experimental	P=14.309 Δ	14.309	4.218
DS804	ANSYS	P=12.078 Δ	12.078	4.997

As shown in "Table 6" we notice that the exported equations are a number multiplied by deflection this constant number is less than the constant (C) so the constant (C) is divided by factor to represent the enhancement factor (K) so we can consider that the number beside the deflection is a factor called (X) and equal C/K so we can consider the equation will be as following:

The equation become $P_{(kN)} = C/k\,\Delta_{(mm)}$

As we have the value of (C=60.357) we can calculate the value of factor (K), the values are shown in "Table 6". From the previous equation, we found that their direct relation between factor (K) and deflection so the lower the value of this factor, the higher the enhancement of the beam.

So, from (K) values in the table, we found that the beams with welded stirrups have the lowest values, so it confirms our concluded results from previous curves.

7. Conclusions

Based on the experimental and theoretical studies, the subsequent conclusions can be ascertained:

1- The experimental investigation revealed a discernible range of cracking loads, spanning from 54% to 62% of the maximum load capacity for stirrup spacing of 200 mm and 150 mm, respectively. The incorporation of welded stirrups not only augmented the cracking load but also increased the ultimate failure load.

2- A comparative analysis between traditional stirrups (four branches) and welded stirrups demonstrated significant advantages for the latter. Welded stirrups led to a remarkable reduction in deflection by 50.50% and an increase in the ultimate load by 62%. This utilization of welded stirrups significantly reduced beam deflection compared to beams without welded stirrups, concurrently enhancing shear resistance.

3- The application of welded stirrups emerges as a notably efficacious strategy for enhancing shear reinforcement in reinforced concrete hidden beams. This strategy creates an interconnected system with reinforcement (RFT) on both the compression and tension sides, collaboratively enhancing the beam's ability to withstand loads.

4- The nuanced influence of varying distances between stirrups on the effectiveness of hidden beams, especially when considering welding, was observed. The results of tested welded beams exhibited closely aligned outcomes, supporting loads of 155.16 kN and 155.18 kN for 150 mm and 200 mm stirrup spacing, respectively. Importantly, augmenting the distance between welded stirrups proved more beneficial than omitting welding, resulting in a significant reduction in deflection, approximately 47.20%, compared to beams without welding and with a lower stirrup spacing.

5- The parametric study, executed through ANSYS simulations, utilized a solid element (SOLID65) for concrete, Link 180 for reinforcement steel bars, and SOLID185 for steel plate modeling. All beams in the investigation were uniformly modeled as simply supported beams. The outcomes revealed substantial enhancements in hidden beams achieved by increasing compression steel ratios and reducing stirrup spacing, resulting in efficiency increments of 49.19% and 25.90%, respectively. The verification analysis, integral for the precise representation of welding in simulations, preceded a comprehensive comparison between experimental and numerical results, facilitating a holistic understanding of the parametric study. The intricate representation of welding in ANSYS poses challenges rooted in geometric, material, and thermal complexities

associated with welding processes. Accurate modeling mandates addressing nonlinear behavior, capturing residual stresses, and navigating multi-physics interactions, underscoring the pivotal yet intricate nature of this aspect in structural analysis.

6- The employment of a smaller upper RFT diameter, while maintaining the same reinforcement ratio, demonstrated subtle improvements in comparison to adopting larger diameters with fewer bars. The experiment aims to investigate whether increasing the surface area of the upper bars contributes to better load distribution, thereby enhancing the beam's load-bearing capacity. However, to provide a conclusive answer to this question, further extensive experimentation is required in future studies. The sample size in this research may not be sufficient to draw definitive conclusions, emphasizing the need for more extensive research in the future.

7- The unexpected discovery that a reduced stirrup diameter led to an increase in beam efficiency challenges preconceptions. This underscores the need for further exploration, as a solitary specimen fails to provide a conclusive evaluation of this parameter's efficacy.

8- This study has extensively explored specific parameters, establishing the groundwork for future research to delve into more intricate relationships among these factors, thereby fostering a more comprehensive understanding. To guide subsequent investigations, we recommend a focused exploration, particularly examining the impact of reducing stirrup diameter and increasing their quantity. Additionally, future studies should consider augmenting the number of bars in both tension and compression while maintaining the prescribed reinforcement ratio. Of paramount importance is an in-depth examination of welding types and their quality, as they significantly influence the effectiveness of hidden beams in bearing loads—a facet crucial to the contributions of this paper. Numerous other factors, which merit detailed investigation in subsequent studies, are anticipated to contribute to a more nuanced understanding of these beam types.

References

[1] ÖZBEK, E., AYKAC, B., BOCEK, M., YıLMAZ, M. C., MOHAMMED, A. B. K., ER, Ş. B. & AYKAC, S. 2020. Behavior and strength of hidden RC beams embedded in slabs. Journal of Building Engineering, 29, 101130.

[2] BELHAQ, M., HELOU, S. H. & AWAD, R. 2014. Performance based analysis of hidden beams in reinforced concrete structures. MATEC Web of Conferences, 16, 10001.

[3] RASHEED, M. H. F. & AGHA, A. Z. S. 2020. Minimum Depth-Span Ratio of Beams in order to Control Maximum Permissible Deflection. The Open Civil Engineering Journal, 14, 402-414.

[4] IRFAN, N. M. & RAVI, G. 2017. Analytical study on Flexural behaviour of RCC slabs with concealed beams. Using ANSYS. International Research Journal of Engineering and Technology (IRJET), 04, 3094.

[5] HSIUNG, W. & FRANTZ G. C. 1985. Transverse Stirrup Spacing in R/C Beams. Journal of Structure Engineering.

[6] MORSY, S. N., SHERIF G. A., SHOEIB, E. A. & AGAMY, H. M.2018. Experimental Study of Enhancing the Shear Strength of Hidden/Shallow Beams by Using Shear Reinforcement. Proceedings of the 3rd World Congress on Civil, Structural, and Environmental Engineering (CSEE'18), ICSENM 116.

[7] CUI, M., NIE, X., FAN, J., LI, S., LIUFU, J. & HUANG, Z. 2019. Experimental study on the shear performance of RC beams reinforced with welded reinforcement grids. Construction and Building Materials, 203, 377-391.

[8] SUN, L., MA, Q., HAN, F., LIU, Z., LI, J., WANG, P., ZHAO, H. & SUN, J. 2020. Experimental investigation on axial compression behavior of steel reinforced concrete columns with welded stirrups. Engineering Structures, 208.

[9] FAWZY, K. & FAROUK, M. A. 2020. Torsion Strengthening of RC Beams with External Lateral Pressure Using Steel Plates. Iranian Journal of Science and Technology, Transactions of Civil Engineering, 45, 1413-1425.

[10] FAWZY, K. & FAROUK, M. A. 2022. Enhanced Repair Techniques of Corroded Reinforced Concrete Short Columns. Practice Periodical on Structural Design and Construction, 27.

[11] IBRAHIM, Y. E., FAWZY, K. & FAROUK, M. A. 2021. Effect of steel fiber on the shear behavior of reinforced recycled aggregate concrete beams. Structural Concrete, 22, 1861-1872.

[12] Egyptian Standard specification for ordinary Portland cement (ESS 4756.-1–2006), Produced from General Organization for Specification and Quality in Egypt, (2020).

[13] ANSYS, Inc. "ANSYS Mechanical APDL Theory Reference" ANSYS, Inc. Release 19.2.

[14] TAVAREZ F. A. 2001. Simulation of Behaviour of Composite Grid Reinforced Concrete Beams Using Explicit Finite Element Methods., Master of Science Thesis, University of Wisconsin–Madison, Madison, Wisconsin.

[15] SHAH S; SWARTZ S.AND OUYANG C. (1995). Fracture Mechanics of Concrete. John Wiley & Sons, Inc., New York.

[16] BANGASH M. 1989. Concrete Structures Numerical Modeling and Applications. Elsevier Science Publishers Ltd., London, England.

[17] DESAYI P. AND KRISHNAN S. 1964. Equation for the Stress-Strain Curve of Concrete. Journal of the American Concrete Institute, 61:345-350.

[18] GERE J. AND TIMOSHENKO S. 1997. Mechanics of Materials. PWS Publishing Company, Boston, Massachusetts.
[19] ECP-203, Egyptian code of practice for design and construction of reinforced concrete structures. Housing and Building Research Center, Giza, Egypt, 2017.
[20] ACI Committee 318, Building code requirements for structural concrete. American Concrete Institute, 2014.
[21] CSA Committee A23.3, Design of concrete structures, CSA A23.3-04. Rexdale, Ontario, Canada: Canadian Standards Association, 2004.
[22] Eurocode EN 1992, "Design of concrete structures, Part 1: General rules and rules for buildings," Thomas Telford, London, 2004.